Available online at www.sciencedirect.com
ScienceDirect
Proceedings of the Combustion Institute 31 (2007) 2537–2545
Proceedings of the Combustion Institute
www.elsevier.com/locate/proci

# Towards large eddy simulations of flame extinction and carbon monoxide emission in compartment fires

Zhixin Hu [a,b], Yunyong Utiskul [a,b], James G. Quintiere [a], Arnaud Trouve [a,c,*]

[a] Department of Fire Protection Engineering, University of Maryland, College Park, MD 20742, USA
[b] Department of Mechanical Engineering, University of Maryland, College Park, MD 20742, USA
[c] Building and Fire Research Laboratory, National Institute of Standards and Technology, 100 Bureau Drive, Gaithersburg, MD 20899, USA

**Abstract**

The general objective of this research is to adapt current combustion modeling capabilities used in computational fluid dynamics solvers to the treatment of under-ventilated compartment fires. More specifically, we consider in the present study two models proposed to describe: diffusion flame extinction due to air vitiation; and the emission of carbon monoxide (CO) and unburnt hydrocarbon (HC) mass in a compartment fire. The flame extinction model is based on a flammability diagram parametrized in terms of vitiated air properties. The CO/HC mass model is based on: a transport equation for fuel mass; a comparison of this fuel mass to a Burke–Schumann chemical-equilibrium expression; and an interpretation of the difference as a measure of incomplete combustion. Both models are implemented into a large eddy simulation solver developed by the National Institute of Standards and Technology, USA. The models performance is tested via detailed comparisons with an experimental database corresponding to reduced-scale compartment fires. The study considers two cases that correspond to different values of the fire room global equivalence ratio and are representative of strikingly different flame behaviors. The comparative tests serve to evaluate the general ability of the models to describe the transition from extinction-free conditions to conditions in which the flame experiences partial or total quenching, as well as the transition from fire regimes with no or little CO emission to regimes that emit hazardous levels.


*Keywords:* Compartment fire; Under-ventilated combustion; Flame extinction; Carbon monoxide emission; Large eddy simulation

## 1. Introduction

The focus of the present study is the near-or post-flashover stages of building compartment fires [1–3]. Near-or post-flashover stages in compartment fires exhibit unique features associated with smoke accumulation and restricted air ventilation. In typical large fire situations, the smoke layer spreads over most of the compartment volume, so that large sections of the flame are supplied with vitiated air, *i.e.* a mixture of pure air and re-circulating combustion products. Air vitiation results in global and local modifications of the flame structure. For instance, if the global

* Corresponding author. Fax: +1 301 405 9383.
*E-mail address:* atrouve@eng.umd.edu (A. Trouve).

1540-7489/$ - see front matter © 2006 The Combustion Institute. Published by Elsevier Inc. All rights reserved.
doi:10.1016/j.proci.2006.08.053

equivalence ratio (GER) in the fire room becomes larger than unity, the flame may experience a dramatic change and migrate from the fuel source to the compartment vents location. This transition is similar to the flame opening process observed in Burke–Schumann-type laminar diffusion flames when going from over- to under-ventilated conditions [4,5].

In addition to these global effects, air vitiation also affects the local values of the flame burning intensity. As discussed in Ref. [6], air vitiation has the double effect of changing the oxidizer stream composition (a dilution effect) as well as its temperature (a pre-heating effect). The net effect of air vitiation is to decrease the heat release rate; and sufficient levels of air vitiation will result in sub-critical oxygen concentrations and consequent flame extinction.

The issue of flame extinction is also related to that of incomplete combustion. In hood or compartment fire experiments, products of incomplete combustion (carbon monoxide, unburnt hydrocarbons, hydrogen) are observed for sufficiently large degrees of air vitiation [7–10], typically when the configuration GER is above 0.5, or equivalently when the oxygen mass fraction inside the (compartment or hood) ceiling layer falls below a critical value called the lower oxygen index. Typical values of the lower oxygen index are 10–15% and depend on fuel type [11,12]. The presence of products of incomplete combustion in the ceiling layer may be explained by flame extinction phenomena occurring in some sections of the flame.

As explained in Ref. [8], flame extinction is only one among several mechanisms that are believed to play a role in the net emission of carbon monoxide from compartment fires. Under over-ventilated conditions, flame extinction events result in unburnt fuel mass leaking through the flame into the ceiling layer; this leaking fuel mass corresponds primarily to carbon monoxide (CO) and unburnt hydrocarbons (HC) species. Depending on the ceiling layer temperatures (*i.e.* for temperatures above 800 K), CO and HC species may also react with ambient residual oxygen, via secondary chemical reactions occurring in the bulk of the ceiling layer [8,13,14].

Similarly, under ventilation-limited conditions, flame extinction events result in air mass being entrained directly into the fuel-rich ceiling layer [8]. Depending on the ceiling layer temperatures (*i.e.* above 800 K), leaking oxygen species may then react with ambient residual unburnt fuel, and thereby augment CO formation [8,13,14]. In addition to these mechanisms, it is worth noting that CO and HC species are natural products of under-ventilated combustion systems, even in the absence of flame extinction. This flame-based mechanism has been documented for instance in fundamental studies of under-ventilated, normal or inverse, laminar diffusion flames [4,5,15].

In summary, the list of mechanisms that contribute to CO formation in compartment fires includes: (1) flame extinction; (2) bulk chemical kinetics in the hot ceiling layer; (3) flame-based kinetics in an under-ventilated configuration. From a modeling perspective, the question of how to adapt computational fluid dynamics (CFD) capabilities in order to treat the full range of CO-mechanisms observed in compartment fires remains entirely open (see Refs. [16,17] for previous attempts). Mechanism (3) may be described using a classical flamelet approach; mechanism (1) may be described using an extended flamelet approach, enhanced by an extinction capability; mechanism (2) corresponds to non-flamelet kinetically-controlled processes, and requires a description of CO chemistry as distributed reactions.

The objective of the present study is to adapt current CFD capabilities to a numerical treatment of flame extinction and CO formation in under-ventilated compartment fires. The developments and tests presented hereafter are made in the context of a CFD solver called the fire dynamics simulator (FDS). FDS is developed by the National Institute of Standards and Technology, USA, and is oriented towards fire applications; it uses a large eddy simulation (LES) approach for turbulence (based on the classical Smagorinsky model) and an equilibrium-chemistry model for non-premixed combustion [18,19].

The latest version of FDS includes a new optional modification to the equilibrium-chemistry combustion model: this modification allows for a description of local flame extinction due to air vitiation [18]. The present study is a continuation of this earlier FDS modeling work and an extension to the problem of CO/HC modeling. The proposed CO/HC model is described in Section 2. Model performance is then evaluated in Section 3 via detailed comparisons with an experimental database corresponding to a reduced-scale compartment [20,21]. The experimental database has been used previously in a series of FDS simulations in which flame extinction and CO formation were ignored [22]. The present study is also a continuation of Ref. [22].

## 2. LES modeling of flame extinction and CO/HC emissions

### 2.1. Modeling of flame extinction due to air vitiation

We start from the equilibrium chemistry model proposed in FDS, in the absence of flame extinction. This model is based on the classical Burke–Schumann theory of diffusion flames in which infinitely fast chemistry is assumed and

the flame structure is described in terms of mixture fraction. It is worth emphasizing that in many fire problems, the turbulent motions are buoyancy-driven and the turbulence intensities remain low-to-moderate. Under such conditions, and assuming well-ventilated conditions, flame extinction remains unlikely and the assumption of infinitely fast chemistry is an acceptable simplification. The model expression for the LES-filtered heat release rate (HRR) per unit volume is:

$$\overline{\dot{q}_{\mathrm{d}}^{\mathrm{eq}}} = \left(\frac{Y_{\mathrm{F}}^{\infty}}{1 - Z_{\mathrm{st}}}\right)\left(\bar{\rho}\frac{\nu_{\mathrm{t}}}{Sc_{\mathrm{t}}}\left|\nabla\widetilde{Z}\right|^{2}\right)\delta(\widetilde{Z} - Z_{\mathrm{st}})\Delta H_{\mathrm{F}} \tag{1}$$

where $Y_{\mathrm{F}}^{\infty}$ is the fuel mass fraction in the fuel supply stream, $Z_{\mathrm{st}}$ the stoichiometric value of mixture fraction $Z$, $\rho$ the mass density, $\nu_{\mathrm{t}}$ the turbulent eddy-diffusivity, $Sc_{\mathrm{t}}$ a turbulent Schmidt number, $\Delta H_{\mathrm{F}}$ the heat of combustion, and where the overbar (tilde) symbol denotes straight (Favre-weighted) LES-filtered quantities. The $\widetilde{Z}$-gradient term on the right-hand side of Eq. (1) represents the LES-filtered rate of fuel-air mixing; the δ-function term represents the stoichiometric value of the probability density function (Pdf) that describes subgrid-scale variations in $Z$. The mixing rate has been expressed using a classical closure expression for the unconditional scalar dissipation rate. The subgrid-scale $Z$-Pdf has been approximated using a crude presumed Pdf approach, in which subgrid-scale variations in $Z$ are simply neglected [23].

We now turn to an extension of the HRR expression in Eq. (1) to cases with flame extinction. The reduction in flame strength resulting from smoke-air mixing is incorporated into the model via the introduction of a flame extinction factor FEF:

$$\overline{\dot{q}_{\mathrm{d}}} = \overline{\dot{q}_{\mathrm{d}}^{\mathrm{eq}}} \times (1 - \mathrm{FEF}) \tag{2}$$

where FEF is the locally defined probability of finding inactive flame elements in a given LES computational grid cell. FEF = 0 (=1) for a fully burning (extinguished) flame.

The model formulation for FEF uses the following ingredients: a critical flame temperature $T_{\mathrm{c}}$, below which extinction is predicted to occur; a lower oxygen index, that characterizes limiting oxygen levels for flames supplied with diluted air at ambient temperature, $T_{\infty} = 300$ K; and a model for the flame temperature $T_{\mathrm{st}}$. The critical flame temperature model may be viewed as a simplified version of a classical description based on critical values of the scalar dissipation rate [24–26]; we use $T_{\mathrm{c}} \approx 1700$ K [27]. The lower oxygen index is also described as an empirical input quantity and is specified as $Y_{\mathrm{O}_2,\mathrm{c}} \approx 0.17$ (mass fraction) [11,12]. The flame temperature model is based on a classical Burke–Schumann expression:

$$T_{\mathrm{st}} = T_1\frac{Y_{\mathrm{O}_2,2}}{r_{\mathrm{s}}Y_{\mathrm{F},1} + Y_{\mathrm{O}_2,2}} + T_2\frac{r_{\mathrm{s}}Y_{\mathrm{F},1}}{r_{\mathrm{s}}Y_{\mathrm{F},1} + Y_{\mathrm{O}_2,2}} + \frac{\Delta H_{\mathrm{F}}}{c_{\mathrm{p}}}\frac{Y_{\mathrm{F},1}Y_{\mathrm{O}_2,2}}{r_{\mathrm{s}}Y_{\mathrm{F},1} + Y_{\mathrm{O}_2,2}} \tag{3}$$

where $T_1$ and $T_2$ are the temperatures in the fuel and oxidizer streams feeding the flame, $Y_{\mathrm{F},1}$ and $Y_{\mathrm{O}_2,2}$ the mass fractions of fuel and oxygen in those feeding streams, $r_{\mathrm{s}}$ the stoichiometric oxygen-to-fuel mass ratio, and $c_{\mathrm{p}}$ the specific heat of the reactive mixture at constant pressure (assumed constant). Equation (3) provides a useful expression of $T_{\mathrm{st}}$ as a function of the oxidizer stream properties $Y_{\mathrm{O}_2,2}$ and $T_2$.

Next, we combine the flame temperature model in Eq. (3) with the concepts of a critical temperature $T_{\mathrm{c}}$ and an oxygen limit $Y_{\mathrm{O}_2,\mathrm{c}}$. We get after some algebraic manipulations:

$$T_{\mathrm{st}} = T_{\mathrm{c}} + (T_{\mathrm{c}} - T_{\infty}) \times \frac{r_{\mathrm{s}}Y_{\mathrm{F},1}}{r_{\mathrm{s}}Y_{\mathrm{F},1} + Y_{\mathrm{O}_2,2}}\left(\frac{Y_{\mathrm{O}_2,2}}{Y_{\mathrm{O}_2,\mathrm{c}}} - \frac{(T_{\mathrm{c}} - T_2)}{(T_{\mathrm{c}} - T_{\infty})}\right) \tag{4}$$

where $T_1 = T_{\infty}$ has been assumed. This expression may now be conveniently used to construct a flammability diagram in terms of the vitiated air variables $Y_{\mathrm{O}_2,2}$ and $T_2$ (Fig. 1). In Fig. 1, non-flammable (flammable) conditions correspond to sub-critical (super-critical) flame temperatures, *i.e.* flame temperatures such that $T_{\mathrm{st}} \leqslant T_{\mathrm{c}}$ ($T_{\mathrm{st}} \geqslant T_{\mathrm{c}}$), or $(Y_{\mathrm{O}_2,2}/Y_{\mathrm{O}_2,\mathrm{c}}) - (T_{\mathrm{c}} - T_2)/(T_{\mathrm{c}} - T_{\infty}) \leqslant 0$ ($\geqslant 0$). And the following binary expression for the flame extinction factor is obtained:

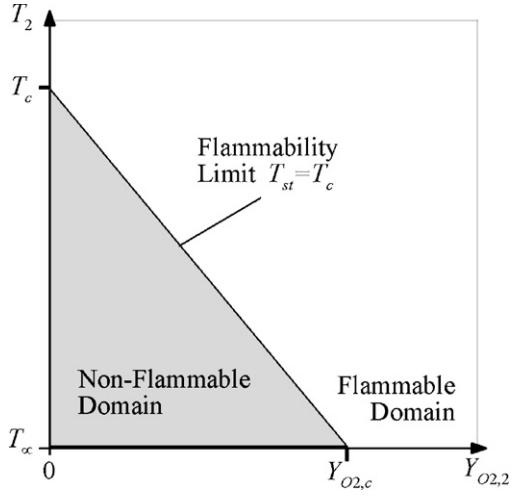


Fig. 1. Flammability diagram for a pure-fuel/vitiated-air diffusion flame, as a function of the vitiated air properties $Y_{\mathrm{O}_2,2}$ and $T_2$, as predicted by the criterion in Eq. (5). The white region corresponds to FEF = 0; the grey region to FEF = 1.

$$\mathrm{FEF} = H\left(\frac{(T_c - T_2)}{(T_c - T_\infty)} - \frac{Y_{O_2,2}}{Y_{O_2,c}}\right) \quad (5)$$

where $H$ is the Heaviside function, $H(x) = 1$ if $x \geqslant 0$, $H(x) = 0$ if $x < 0$.

Equation (5) is a closure model for FEF, provided that the variables $Y_{O_2,2}$ and $T_2$ are known. Note that the oxidizer stream properties correspond to unresolved conditional information, and should not be confused with the LES grid-resolved oxygen mass fraction and temperature, $\widetilde{Y}_{O_2}$ and $\widetilde{T}$. The estimation of $Y_{O_2,2}$ and $T_2$ in Eq. (5) is based on a simple search algorithm applied to all computational grid cells in which heat release is taking place. The search algorithm interrogates neighboring cells and identifies among them the cells that are both non-reacting ($\dot{q}_d^{eq} = 0$) and located on the lean side of the flame ($\widetilde{Z} \leqslant Z_{st}$); the values of $\widetilde{Y}_{O_2}$ and $\widetilde{T}$ in those oxidizer cells are then used to estimate the vitiated air conditions at the LES flame location. With this scheme, Eqs. (2) and (5) provide an extended HRR model.

### 2.2. Modeling of CO/HC mass

We now turn to a description of the CO/HC mass. This description is based on a transport equation for the LES-filtered fuel mass fraction $\widetilde{Y}_F$ (which includes flame extinction effects) and a comparison between $\widetilde{Y}_F$ and the Burke–Schumann fuel mass fraction $Y_F^{eq}(\widetilde{Z})$ that would be obtained under equilibrium conditions (*i.e.* in the absence of flame extinction). We write:

$$\frac{\partial}{\partial t}(\bar{\rho}\widetilde{Y}_F) + \frac{\partial}{\partial x_i}(\bar{\rho}\widetilde{u}_i\widetilde{Y}_F) = \frac{\partial}{\partial x_i}\left(\bar{\rho}\left(\frac{\nu}{Sc_F} + \frac{\nu_t}{Sc_t}\right)\frac{\partial \widetilde{Y}_F}{\partial x_i}\right) + \overline{\dot{\omega}_F^{eq}} \times (1 - \mathrm{FEF}) \quad (6)$$

where $u_i$ is the $x_i$-component of the flow velocity vector, $\nu$ the kinematic viscosity, $Sc_F$ a Schmidt number, and where $\dot{\omega}_F^{eq}$ is the LES-filtered fuel mass reaction rate obtained in the infinitely fast chemistry limit. We note that in this limit, chemical reaction is confined to the stoichiometric fuel-air surface, and $\widetilde{Y}_F$ remains 0 on that surface. In other words, the chemical sink term $\overline{\dot{\omega}_F^{eq}}$ must balance exactly convection and diffusion transport of incoming fuel. Using Eq. (6), we may write:

$$\overline{\dot{\omega}_F^{eq}} = \frac{\partial}{\partial x_i}(\bar{\rho}\widetilde{u}_i\widetilde{Y}_F) - \frac{\partial}{\partial x_i}\left(\bar{\rho}\left(\frac{\nu}{Sc_F} + \frac{\nu_t}{Sc_t}\right)\frac{\partial \widetilde{Y}_F}{\partial x_i}\right) \quad (7)$$

which holds at the LES flame surface location, *i.e.* at $\widetilde{Z} = Z_{st}$.

While attractive because of its simplicity, while also compliant with global mass conservation requirements, the model expression in Eq. (7) is affected by numerical stiffness problems: the thickness of the reaction zone corresponds to a single computational grid cell. The model is therefore prone to numerical diffusion errors. While improvements are possible [23], we choose to work in the following with the model as formulated in Eqs. (6) and (7).

Next, we discuss the implications of the fuel mass model for CO predictions. The idea here is to compare the fuel mass obtained using the model in Eqs. (6,7) with that obtained using the classical Burke–Schumann equilibrium-chemistry model, $Y_F^{eq}(\widetilde{Z}) = 0, \widetilde{Z} \leqslant Z_{st}; Y_F^{eq}(\widetilde{Z}) = Y_F^{\infty}(\widetilde{Z} - Z_{st})/(1 - Z_{st}), \widetilde{Z} \geqslant Z_{st}$ [24–26], and simply interpret the deviations of $\widetilde{Y}_F$ from $Y_F^{eq}(\widetilde{Z})$ as a measure of incomplete combustion. We write:

$$\widetilde{Y}_{CO+HC} = \widetilde{Y}_F - Y_F^{eq}(\widetilde{Z}) \quad (8)$$

where $\widetilde{Y}_{CO+HC}$ designates the mass fraction of combined CO and HC species.

Equation (8) is the current model expression used to provide information on CO emissions. We consider Eq. (8) as an intermediate stage on the route of CO predictions; for instance, the fact that the variable $\widetilde{Y}_{CO+HC}$ does not differentiate between CO and HC mass remains a significant problem since both carbon monoxide and unburnt hydrocarbons are produced in large quantities in under-ventilated compartment fires [7–10]. Also, as mentioned above, the modeling of $\widetilde{Y}_F$ based on Eq. (7) remains crude. In the following, we accept these limitations and proceed to perform validation tests of the current formulation. The validation tests are based on FDS simulations of a reduced-scale compartment fire configuration.

## 3. LES simulations of a small-scale compartment fire experiment

### 3.1. Experimental configuration

The experimental set-up corresponds to a reduced-scale compartment that communicates to the exterior through an adjustable wall vent arrangement (Fig. 2). The compartment size is $(40 \times 40 \times 40)$ cm$^3$. The wall vent arrangement consists of two vents of equal size located at the top and bottom of one of the compartment vertical walls. The vents width varies between 2 and 40 cm; the vents height varies between 1 and 3 cm. The fire is fueled by a round-shaped heptane pool located at the center of the compartment floor. The fuel pans are containers of different size, with diameters ranging from 6.5 to 19 cm.

The compartment is instrumented with sensors and probes that provide the time history of the fuel mass loss rate (MLR), of local temperatures and surface heat fluxes at different locations, and of local floor- and ceiling-level concentrations of

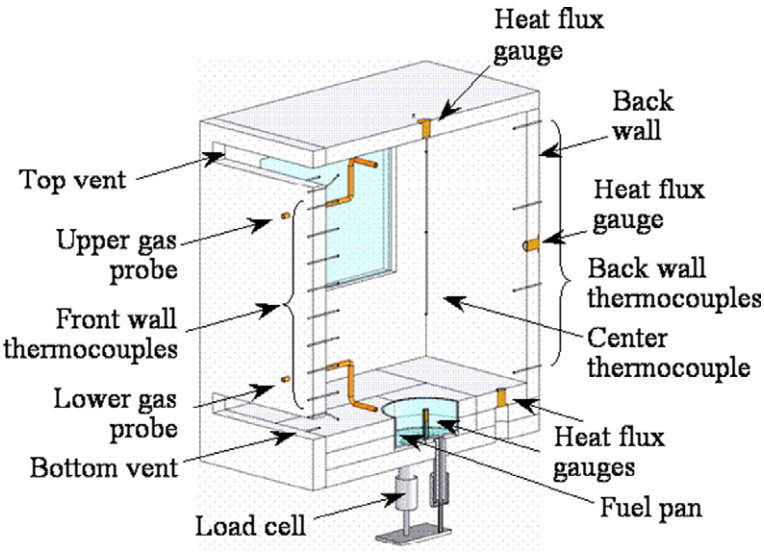


Fig. 2. Schematic half-view of the experimental configuration. In our choice of coordinates, $z$ measures vertical elevation; $x$ and $y$ measure horizontal distance from the center of the fuel pan ($x = 0.2$ is the vented wall location).

important chemical species, such as $O_2$, $CO_2$ and CO. Details about the compartment instrumentation may be found in Refs. [20,21].

A wide variety of flame behaviors is observed in the experimental database, as reported in Refs. [20,21]. These flame behaviors belong to one of the following four categories [22]: (R1) steady well-ventilated fires in which the flame is stabilized above the burner; (R2) steady under-ventilated fires in which the flame is stabilized near the vents; (R3) unsteady under-ventilated fires featuring large periodic oscillations and temporary flame quenching; (R4) unsteady under-ventilated fires leading to complete flame extinction. The main parameter that controls transition from one flame regime to the other has previously been identified as the fire room GER. In short, regime R1 corresponds to small values of GER; regime R4 to large values of GER; and regimes R2 and R3 to intermediate, near-stoichiometric values.

It is worth noting that in small-scale compartment fires, the weight of thermal losses experienced by the fire gases is somewhat artificially increased, and ceiling layer temperatures are typically lower than those observed in large full-scale tests. In the experimental database of Refs. [20,21], ceiling layer temperatures remain below 800–900 K. These moderate temperature levels are below those required for the activation of the kinetically-controlled CO formation mechanism (mechanism (2)) discussed in Section 1.

Also, we focus our discussion in Section 3.3 on two cases from the experimental database, cases 2 and 4 in the nomenclature adopted in Ref. [22]. The two cases differ due to variations in vent size and fuel surface area; the cases are representative of the flame regimes R2 and R4 listed above; they are also representative of mechanisms (1) and (3) of CO formation.

### 3.2. Numerical configuration

The calculations are performed using FDS, Version 4.05 [18]. The computational domain corresponds to two non-overlapping blocks of equal size, corresponding to the fire compartment and to the adjacent exterior air space. The computational grid in each block corresponds to a uniform rectangular mesh; the mesh size is $(80 \times 80 \times 80)$, which corresponds to cubic grid cells with a 0.5 cm spacing. Further details about the design and suitability of the numerical configuration and computational grid may be found in Ref. [22]. Simulations are performed on a multi-processor Linux machine, using the parallel MPI-based version of FDS.

Note that the FDS calculations correspond here to a simplified treatment of the fuel mass loss rate: a prescribed-MLR treatment in which the time history of MLR is directly taken from the experimental database and treated as an input variable.

### 3.3. Results

We start our discussion with case 2 and compare the experimental data to the prescribed-MLR computational results (Fig. 3). Case 2 is representative of regime R2 in which the combustion becomes oxygen-limited, and the flame

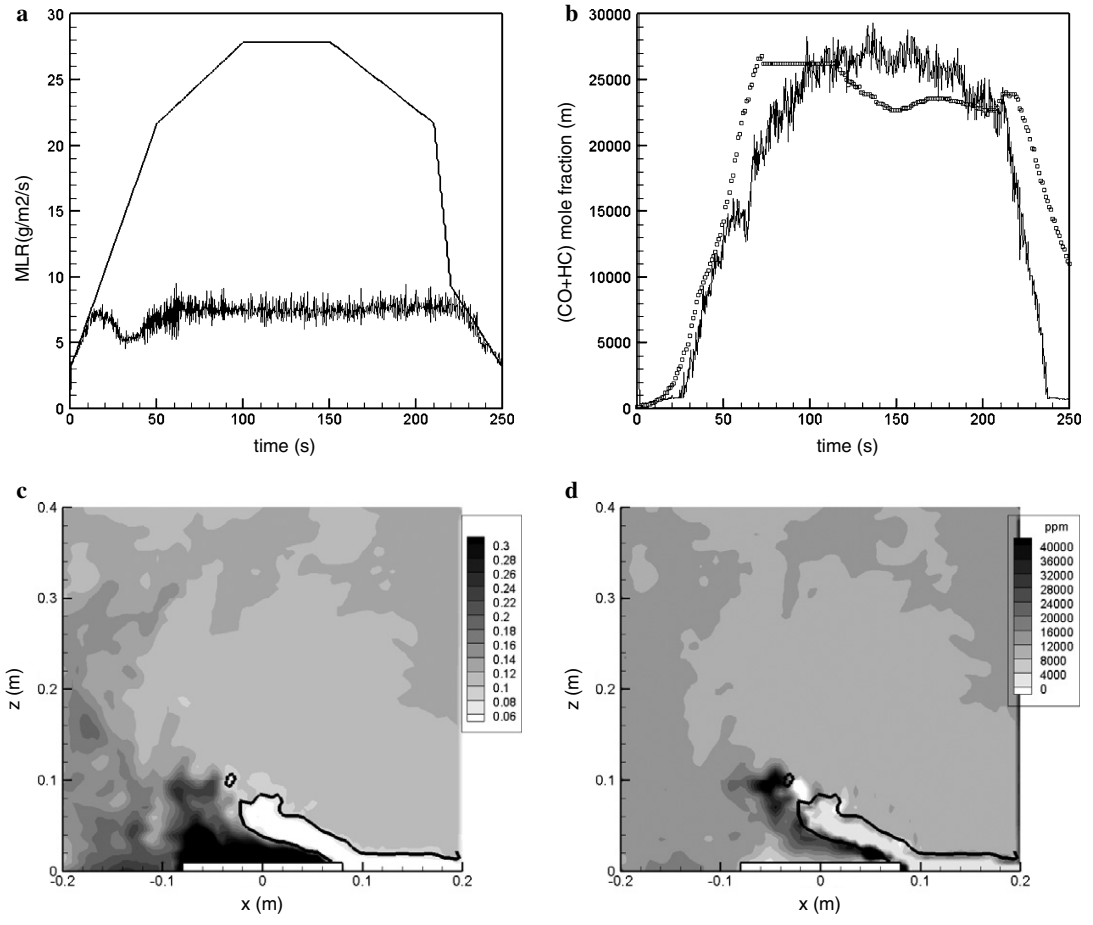


Fig. 3. Case 2: vent height × width = 1 × 40 cm$^2$; fuel pan diameter = 16 cm. Fig. 3a: experimental MLR (piecewise linear line) and simulated BR (oscillating line) *vs* time. Fig. 3b: experimental CO mole fraction (symbols) and simulated (CO/HC) mole fraction (solid line) *vs* time, near-ceiling location. Bottom plots: instantaneous isocontour plots of simulated $\widetilde{Z}$ (Fig. 3c) and $\widetilde{Y}_{\mathrm{CO+HC}}$ (Fig. 3d), $y = 0$ plane, $t = 100$ s. The fuel pan is visualized as a white rectangle located at floor level at $-0.08 \leqslant x \leqslant 0.08$ m.

detaches from the fuel pan and successfully stabilizes near the compartment lower vent. In the fully-developed stage of the fire, GER $\approx 3.5$. Figure 3a indicates that the fuel MLR (per unit surface area) increases to approximately 25 g/s/m$^2$. Note that the total mass of heptane used in the experiment is finite, and that given the observed value of MLR, the burn duration is approximately 250 s.

Figure 3a also compares the time variations of MLR with those of the burning rate BR; the burning rate is defined as: $\mathrm{BR} = (\int\int\int_V \overline{\dot{q}_{\mathrm{d}}}\, \mathrm{d}V)/(\Delta H_{\mathrm{F}} A_{\mathrm{F}})$, where $V$ is the volume of the compartment and $A_{\mathrm{F}}$ the fuel source area; BR is obtained from the LES solution. Under over-ventilated fire conditions, and in absence of flame extinction, the totality of the vaporized fuel mass is consumed by the turbulent flame and in a time-averaged sense, BR $\approx$ MLR. In contrast, under oxygen-limited conditions, the flame cannot consume all the incoming fuel, and excess fuel mass either accumulates in the fire room or is convected out through the upper vent. Under such conditions, BR $<$ MLR. Previous simulations performed without flame extinction [22] have shown that transition from over- to under-ventilation takes place at time $t \approx 30$ s. Also, comparisons between simulations performed with and without flame extinction suggest that in case 2, the impact of flame extinction is limited to transient quasi-stoichiometric fire conditions, around $t \approx 30$ s (during fire growth) and $t \approx 230$ s (during fire decay). In the fully-developed stage of the fire, the flame is located near the lower vent and is simply not exposed to vitiated air.

Figure 3c presents an instantaneous snapshot of mixture fraction taken from the LES solution. The snapshot is taken at an arbitrarily chosen time and the isocontours are plotted in the central vertical plane of the compartment that cuts through the fuel pan and the vents. The stoichiometric isocontour ($Z_{st} \approx 0.062$) may be used to identify the LES flame location: in Fig. 3c, this contour is highlighted as a black solid line. It is seen that the flame now stands away from the fuel pan and in the proximity of the air stream coming in through the lower vent.

Figure 3b presents the time variations of CO mole fraction, as measured from the ceiling-level probe (Fig. 2), and compares these variations to those of the simulated combined CO/HC mass. It is seen that the CO levels are quite high for this case, up to approximately 3%. As previously discussed, once located at the lower vent, the flame is well-ventilated and remains extinction-free. We therefore believe that the CO mass in Fig. 3b is produced by the flame-based kinetics mechanism (mechanism (3)) discussed in Section 1. Note also that (while keeping in mind that the plotted quantities are different) the computational results show reasonable agreement with the experimental data.

Figure 3d presents an instantaneous snapshot of the simulated CO/HC mass, in a plane and at a time that are identical to those used in Fig. 3c. Peak CO values are found to occur in the flame region. In case 2, the CO produced at the flame remains insulated from the air stream and simply accumulates in the ceiling layer with no further chance to get oxidized.

We now turn to case 4 (Fig. 4). Case 4 is representative of regime R4 in which the combustion experiences complete extinction. The asymptotic steady-state value of GER is above 10. Figure 4a indicates that the fuel MLR abruptly decreases at time $t \approx 40$ s; at this time, GER $\approx 1$ [22], *i.e.* the fire remains over-ventilated up to extinction (and never achieves the asymptotic GER value). Comparisons between simulations performed with

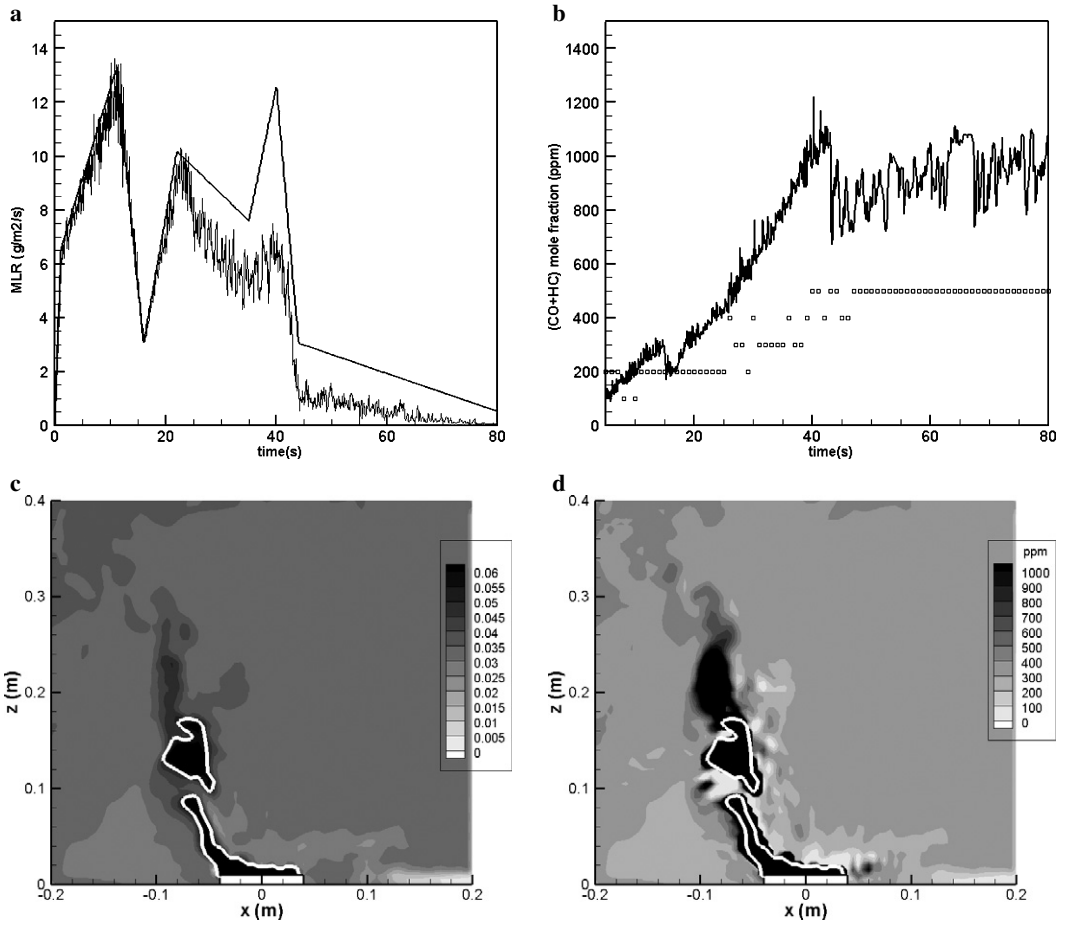


Fig. 4. Case 4: vent height × width = $1 \times 2$ cm$^2$; fuel pan diameter = 8 cm. See Fig. 3 for details. Bottom plots: $t = 35$ s. The fuel pan is visualized as a white rectangle located at floor level at $-0.04 \leqslant x \leqslant 0.04$ m.

and without flame extinction suggest that in case 4, flame extinction events play a dominant role and account for the differences between MLR and BR observed in Fig. 4a. For $t \geqslant 20$ s, about half of the fuel mass that is vaporized does not burn, and total quenching is observed before MLR goes to 0.

Figure 4c presents an isocontour plot that is similar to Fig. 3c, with the difference that a different range of isolevels has been selected and that the flame contour is now highlighted as a white solid line. At $t = 35$ s, the flame features a classical cone-like shape, and is attached to the fuel pan.

Figure 4b presents the CO data at the ceiling-level probe location. It is seen that the CO levels are much lower than in case 2, and are on the order of a few hundred ppm. Note that the resolution of the CO gas analyzer is 100 ppm and as a result, the CO measurements display step-like variations in Fig. 4b. As mentioned above, the flame remains over-ventilated in case 2 but is also overwhelmed by flame extinction. We therefore believe that the CO mass in Fig. 4b is produced by the flame extinction mechanism (mechanism (1)) discussed in Section 1. The computational results are seen to over-predict the experimental measurements, a result that may still be acceptable since the LES model provides information on combined CO/HC mass, while the gas analyzer measures CO only.

Figure 4d presents the spatial distribution of $\widetilde{Y}_{\mathrm{CO+HC}}$ at $t = 35$ s. Peak CO values are found to occur in the flame region. The CO/HC mass that leaks through the flame at extinction locations accumulates in the ceiling layer before being convected away through the upper vent.

## 4. Conclusion

The present study is aimed at adapting current LES capabilities to a description of under-ventilated compartment fires, with an emphasis on air vitiation effects and CO formation. Two new models are considered: a flame extinction model based on a flammability diagram parametrized in terms of vitiated air properties; a CO/HC mass model based on a transport equation for fuel mass, and a comparison of this fuel mass to a Burke–Schumann chemical-equilibrium expression. The new models are tested via detailed comparisons with an experimental database corresponding to a reduced-scale compartment fire configuration.

Two cases are studied in detail; these cases correspond to a steady under-ventilated fire in which the flame is stabilized near the vents (case 2 in our nomenclature), and an unsteady under-ventilated fire leading to complete flame extinction (case 4). CO formation in case 2 is believed to be dominated by a mechanism associated with flame-based kinetics; this mechanism is similar to that responsible for CO emissions in under-ventilated, normal or inverse, laminar diffusion flames. CO formation in case 4 is believed to be dominated by flame extinction. The comparisons between computational results and experimental data are found to be encouraging, although the CO formation model remains qualitative in many ways. The model also remains limited in scope since it neglects an additional CO formation mechanism that corresponds to distributed reaction in the hot ceiling layer.

## Acknowledgments

This work is supported by the U.S National Institute of Standards and Technology, Building and Fire Research Laboratory. Interactions with our contract monitors, A. Hamins and K. McGrattan, are gratefully acknowledged.

## References

[1] D. Drysdale, *An Introduction to Fire Dynamics*, second ed., John Wiley & Sons, 1998.
[2] B. Karlsson, J.G. Quintiere, *Enclosure Fire Dynamics*, CRC Press LLC, 2000.
[3] J.G. Quintiere, *Proc. Combust. Inst.* 29 (2002) 181–193.
[4] S. Leonard, G.W. Mulholland, R. Puri, R.J. Santoro, *Combust. Flame* 98 (1994) 20–34.
[5] M.P. Tolocka, P.B. Richardson, J.H. Miller, *Combust. Flame* 118 (1999) 521–536.
[6] J.G. Quintiere, A.S. Rangwala, *Fire Mat.* 28 (2003) 387–402.
[7] C.L. Beyler, in: Proceedings of First International Symposium, International Association for Fire Safety Science, Hemisphere Publishing Corporation, 1986, pp. 431-440.
[8] W.M. Pitts, *Prog. Energy Combust. Sci.* 21 (1995) 197–237.
[9] A. Tewarson, *Toxicology* 115 (1996) 145–156.
[10] D.T. Gottuk, B.Y. Lattimer, *SFPE Handbook of Fire Protection Engineering*, National Fire Protection Association, third ed., 2002, 2/54–2/82.
[11] G. Mulholland, M. Janssens, S. Yusa, W. Twilley, V. Babrauskas, in: Proceedings of Third International Symposium, International Association for Fire Safety Science, Elsevier Science Publishers, 1991, pp. 585-594.
[12] J.H. Morehart, E.E. Zukoski, T. Kubota, *Fire Saf. J.* 19 (1992) 177–188.
[13] W.M. Pitts, *Proc. Combust. Inst.* 24 (1992) 1737–1746.
[14] D.T. Gottuk, R.J. Roby, C.L. Beyler, *Fire Saf. J.* 24 (1995) 315–331.
[15] L.G. Blevins, R.A. Fletcher, B.A. Benner, E.B. Steel, G.W. Mulholland, *Proc. Combust. Inst.* 29 (2002) 2325–2333.
[16] W.M. Pitts, in: Proceedings of Fifth International Symposium, International Association for Fire

Safety Science, Hemisphere Publishing Corporation, 2004, pp. 535-546.
[17] S.M. Hyde, J.B. Moss, in: Proceedings of Seventh International Symposium, International Association for Fire Safety Science, 2003, pp. 395–406.
[18] K.B. McGrattan, National Institute of Standards and Technology NIST Special Publication 1018, Gaithersburg, MD, 2004.
[19] K. McGrattan, J. Floyd, G. Forney, H. Baum, S. Hostikka, in: Proceedings of Seventh International Symposium, International Association for Fire Safety Science, 2003, pp. 827–838.
[20] Y. Utiskul, J.G. Quintiere, T. Naruse, in: Proc. Tenth Intl. Interflam Conf. InterScience Communications (2004) 105–116.
[21] Y. Utiskul, J.G. Quintiere, A.S. Rangwala, B.A. Ringwelski, K. Wakatsuki, T. Naruse, *Fire Saf. J.* 40 (2005) 367–390.
[22] Z. Hu, Y. Utiskul, J.G. Quintiere, A. Trouvé, in: Proceedings of the Eighth International Symposium Fire Safety Science, International Association for Fire Safety Science, 2005, pp. 1193–1204.
[23] Z. Hu, G. Panafieu, J. Stauder, A. Trouvé, in: Proceedings in Congress on Computational Simulation Models in Fire Engineering and Research, University of Cantabria, Santander, Spain, 2004, pp. 281–295.
[24] F.A. Williams, *Combustion Theory*, second ed., Benjamin/Cummings, 1985.
[25] D. Veynante, L. Vervisch, *Prog. Energy Combust. Sci.* 28 (2002) 193–266.
[26] T. Poinsot, D. Veynante, *Theoretical and Numerical Combustion*, second ed., Edwards, 2004.
[27] C. Beyler, *SFPE Handbook of Fire Protection Engineering*, National Fire Protection Association, third ed., 2002, pp. 2–172, 2–187.

## Comment

*Matthew Cleary, Imperial College, UK.* Have you done any numerical modeling of the enclosures of heat fires to see if you can predict CO rise near a GER of 0.5 and plateau for GER > 2? Is temperature a function of mixture fraction? Do you account for heat loss due to radiation?

*Reply.* With respect to your first question, we are currently performing a new series of simulations that correspond to classical hood experiments taken from the literature with the intent of reproducing the increase in CO yield observed for values of the global equivalence ratios (GER) above 0.5 and the approximately constant value of the CO yield observed for GER values above 2. We agree that these simulations are a key step in establishing the performance of the CO formation model.

With respect to your second question, temperature is not a sole function of mixture fraction as it is also determined by convective and radiative heat losses.

With respect to your third question, we do account in the simulations for thermal radiation transport via a solution of the radiative transfer equation (RTE). The radiation model used in the present simulations assumes gray gas properties.